Hindawi Publishing Corporation
Journal of Nanomaterials
Volume 2016, Article ID 6502127, 9 pages
http://dx.doi.org/10.1155/2016/6502127

Research Article

Dual-Modality Imaging Probes with High Magnetic Relaxivity and Near-Infrared Fluorescence Based Highly Aminated Mesoporous Silica Nanoparticles

Zhu Fei-Peng,[1,2] Chen Guo-Tao,[3] Wang Shou-Ju,[1] Liu Ying,[1] Tang Yu-Xia,[1] Tian Ying,[1] Wang Jian-Dong,[4] Wang Chun-Yan,[1] Wang Xin,[1] Sun Jing,[1] Teng Zhao-Gang,[1] and Lu Guang-Ming[1]

[1]*Department of Medical Imaging, Jinling Hospital, School of Medicine, Nanjing University, Nanjing 210002, China*
[2]*Department of Medical Imaging, The First Affiliated Hospital with Nanjing Medical University, Nanjing 210029, China*
[3]*Department of Medicine, Nanjing University, Nanjing 210093, China*
[4]*Department of Pathology, Jinling Hospital, School of Medicine, Nanjing University, Nanjing 210002, China*

Correspondence should be addressed to Teng Zhao-Gang; tzg@fudan.edu.cn and Lu Guang-Ming; cjr.luguangming@vip.163.com

Received 13 January 2016; Revised 28 February 2016; Accepted 21 April 2016

Academic Editor: Jorge Pérez-Juste

Dual-modal imaging by combining magnetic resonance (MR) and near-infrared (NIR) fluorescence can integrate the advantages of high-resolution anatomical imaging with high sensitivity in vivo fluorescent imaging, which is expected to play a significant role in biomedical researches. Here we report a dual-modality imaging probe (NIR/MR-MSNs) fabricated by conjugating NIR fluorescent heptamethine dyes (IR-808) and MR contrast agents (Gd-DTPA) within highly aminated mesoporous silica nanoparticles (MSNs-NH_2). The dual-modality imaging probes NIR/MR-MSNs possess a size of ca. 120 nm. The NIR/MR-MSNs show not only near-infrared fluorescence imaging property with an emission peak at 794 nm, but also highly MR T_1 relaxivity of 14.54 mM^{-1} s^{-1}, which is three times more than Gd-DTPA. In vitro experiment reveals high uptake and retention abilities of the nanoprobes, while cell viability assay demonstrates excellent cytocompatibility of the dual-modality imaging probe. After intratumor injection with the NIR/MR-MSNs, MR imaging shows clear anatomical border of the enhanced tumor region while NIR fluorescence exhibits high sensitive tumor detection ability. These intriguing features suggest that this newly developed dual-modality imaging probes have great potential in biomedical imaging.

1. Introduction

Magnetic resonance (MR) and near-infrared (NIR) fluorescence have been widely used as powerful imaging tools in biomedical areas [1–6]. However, due to the inherent limitations of MR and NIR, it is still impossible to get molecular, functional, and anatomical information by signal imaging method [1, 2, 7, 8]. In order to take the synergistic advantages of each imaging modality, great efforts have been conducted to explore MR/NIR dual-modal imaging tools [3, 9–13]. For example, NIR dye has been modified onto MR-detectable nanomaterials such as superparamagnetic iron oxide nanoparticles (SPIONs) to build MR/NIR bimodal imaging probe [14–16]. However, the direction modification dyes on the SPIONs indeed do not have many disadvantages. First, the black SPIONs can directly quench the fluorescence of the dye. Second, the emitted fluorescence can also be absorbed by the SPIONs [14, 16]. In addition, surface modifications are commonly needed to connect functional molecules, which makes the SPION based dual-modality probes even more complicated [14]. Another method is conjugating MR agents with semiconductor quantum dots (QDs) [1, 17–19]. Yet, the drawback of the toxicity of heavy cadmium metal makes QD based imaging probes potential clinical usage limited [1].

Recently, mesoporous silica nanoparticles (MSNs) have attracted increasing attention as an ideal matrix to integrate imaging tags to develop imaging probes, due to the high

surface area, uniform pore size, excellent biocompatibility, and no absorption of NIR light or interference with magnetic fields [11, 17, 20, 21]. There have been several reports about MSN based imaging probes [17, 21–23]. Taylor et al. [23] synthesized MSN based nanoparticulate T_1 weighted MR contrast agents with a high r_1 relaxivity by refluxing MSNs and Gd-Si-DTTA complex in toluene. Although rodent experiment confirmed the MR imaging ability of the particles, the authors failed to evaluate the optical fluorescent property in vivo [23]. Sharma et al. [22] produced gadolinium-doped silica nanoparticles by encapsulation indocyanine green with a reverse-microemulsion-based synthesis protocol; both in vitro and in vivo studies showed fine NIR and MR contrast capabilities. However, the protocol is complex and the r_1 relaxivity elevation was only 7.3 mM^{-1} s^{-1} on a 4.7 T MR. Till now, there very few reports on the high MR r_1 relaxivity and NIR imaging probes have been documented.

In this study, we designed and synthesized a novel NIR/MR dual-modality imaging probe (NIR/MR-MSNs) by facile conjugation of NIR fluorescent heptamethine dyes IR-808 and MR contrast agents Gd-DTPA within highly aminated MSNs (MSNs-NH_2) via a one-step procedure. The NIR/MR-MSNs not only were easy to produce, but also possessed uniform particle size, high surface area, and excellent biocompatibility. In vitro cell experiment illustrated high cellular uptake, retention abilities, and excellent biocompatibility of the NIR/MR-MSNs. Excellent NIR fluorescence property and highly efficient MR T_1 contrast effect were also found in in vitro and in vivo imaging studies. Importantly, the NIR/MR-MSNs provide simultaneously clear anatomical border of enhanced tumor region and high sensitive fluorescence imaging. These all suggested that the NIR/MR-MSNs are suitable for potential applications as a useful dual-modality biomedical imaging probes.

2. Materials and Methods

2.1. Materials. Hexadecyltrimethyl ammonium bromide (CTAB), tetraethyl orthosilicate (TEOS), and N-hydroxysulfosuccinimide sodium salt (NHS) were purchased from Sinopharm Chemical Reagent Co. (China). Ethyl ethanoate (EtOAc), ammonium hydroxide in water (25 wt%), and ethyl alcohol were purchased from Nanjing Chemical Reagent Co. (China). 3-Aminopropyltriethoxysilane (APTES) was purchased from Sigma-Aldrich (USA). 1-(3-Dimethylaminopropyl)-3-ethylcarbodiimide hydrochloride (EDC·HCl) was purchased from Aladdin Industrial Inc. (China). 2-(N-Morpholino) ethanesulfonic acid (MES) sodium salt buffer solution was purchased from Thermo Fisher Scientific Inc. (USA). Gd-DTPA was purchased from Guangzhou Consun Pharmaceutical Group Ltd. (China). 3-(4,5-Dimethylthiazol-2-yl)-2,5-diphenyltetrazolium bromide (MTT) was purchased from Sigma-Aldrich (USA). The near-infrared fluorescent heptamethine indocyanine dye (IR-808) was presented by Professor Chun-meng Shi of the Third Military Medical University.

2.2. Synthesis of MSNs-NH_2. MSNs-NH_2 were synthesized according to the previously reported method [24]. In brief, 7.04 mL of ethyl acetate, 24.24 mL of ammonium hydroxide, and 0.8 g of CTAB were added to 1135 mL deionized water and stirred at room temperature until CTAB completely dissolved. Afterward, 1.8 mL of TEOS and 2.2 mL of APTES were added under vigorous stirring. After 24 h, the products were centrifuged and washed with deionized water. Finally, the CTAB was removed by three extractions in 240 mL of ethanol and 480 μL of concentrated hydrochloric acid at 60°C for 3 h.

2.3. Synthesis of Gd/NIR-MSNs. 1 mL of MSNs-NH_2 solution (50 mg/mL), 0.7 mg IR-808, and 4 mL Gd-DTPA aqueous solution (0.1 M) were mixed in MES-NHS buffer and shattered by an ultrasonic cell disrupter for 30 min in dark. Then, EDC·HCl was added in the solution and stirred in dark overnight. The sample was washed with water and redispersed in deionized water.

2.4. Characterization of Gd/NIR-MSNs. Transmission electron microscopy (TEM) images were obtained with a Tecnai G2 F20 microscope (FEI, Hillsboro, OR) at 200 KV. Nitrogen sorption isotherms were obtained with a V-Sorb 2800P physisorption instrument (Gold APP Instrument Corporation, China). Surface areas were calculated according to the Brunauer-Emmett-Teller (BET) method. The pore size distributions were calculated from the adsorption branches of the isotherms according to the nonlocal density functional theory (NLDFT) method. The absorption curve of Gd/NIR-MSNs and loading efficiency of IR-808 were determined by UV-vis spectrum with a UV-vis Lambda 35 (PerkinElmer, USA). To confirm the presence of Gd-DTPA in Gd/NIR-MSNs, electron dispersive X-ray (EDX) was performed using a Tecnai G2 F20 electron microscopy with an EDX detector system. Gd concentration was determined with a Perkin-Elmer OPTIMA 5300 DV (PerkinElmer, USA) inductively coupled plasma atomic emission spectroscopy (ICP-AES). MR examination was performed with a 3 T clinical MR scanner (MAGNETOM Trio, SIMENS, Germany) at room temperature. After acquiring the T_1 map MR images, T_1 values were measured by manually drawn regions of interest for each sample. Relaxation rates $r_1 (r_1 = 1/T_1)$ were calculated from T_1 values at different Gd concentrations.

2.5. Cellular Experiments

2.5.1. Cell Culture. Human embryonic kidney HEK 293T cells were cultured in Roswell Park Memorial Institute (RPMI) 1640 medium (Invitrogen, California, USA) supplemented with 1 mmol/L L-glutamine and 10% fetal bovine serum (FBS; Life Technologies, Inc. Burlington, Canada). Human glioblastoma cell line U87-MG-GFP cells were maintained in Dulbecco's modified eagle medium (DMEM; KeyGEN Bio TECH, Nanjing, China) supplemented with 10% FBS. All media were added with antibiotics (100 U/mL of penicillin G and 100 μg/mL of streptomycin). All cells were incubated at 37°C in a humidified atmosphere of 95% air and 5% CO_2.

2.5.2. In Vitro Fluorescent Microscopy and MR Imaging of U87-MG Cell Labeling with Gd/NIR-MSNs. Green

fluorescent protein (GFP) labeling human glioblastoma cell line U87-MG were passaged 1 day before adding Gd/NIR-MSNs and inoculated in a 24-well chamber slides. After the cells attached to the chamber slides, stock solutions of Gd/NIR-MSNs were centrifuged and redispersed in fresh growth media and added to cultured cells to a final concentration of 0.1 mg/mL. Cells were incubated at 37°C overnight. The next day, label-containing media were aspirated carefully. Cells were washed five times with phosphate buffered saline solution (PBS) to remove excess nanoparticles and fixed with 10% formaldehyde at 4°C. After supernatant removed, 4′,6-diamidino-2-phenylindole (DAPI) was added to each chamber and incubated for 20 min. The slides were then washed three times with PBS and covered with glass coverslips.

Fluorescent images were recorded by a fluorescent inverted microscopy (Olympus, Japan). Imaging of DAPI was carried out with excitation of 330~385 nm and emission at 420 nm, while imaging of GFP was performed with excitation of 460~490 nm and emission of 510 nm. Gd/NIR-MSNs were excited by the external laser at 950 nm, while the emissions were collected in the ranges of 684 to 719 nm. To identify the Gd/NIR-MSNs uptaken by cells, fluorescent microscopy images were overlaid.

To further evaluate the dual-modality imaging ability of the Gd/NIR-MSNs, we designed an in vitro phantom experiment. In brief, U87-MG cells were incubated with Gd/NIR-MSNs or MSNs-NH_2 containing medium at a density of 5×10^6 cells/mL in 6 cm culture dishes at 37°C for 4 h, respectively. And then, the labeled cells were harvested and washed five times by centrifuge to remove additional nanoparticles. NIR imaging was performed using an IVIS Lumina XR system (Xenogen, USA), with the emission collected 808 nm and excited by the external laser at 778 nm. MR T_1 map imaging was performed with a 3.0 T clinical MR scanner and a custom, premade four-channel mouse coil. The parameters were as follows: TR = 15.0 ms, TE = 1.73 ms, Average = 2, Slice Thickness: 2.0 mm, FOV = 113 mm, and Flip Angle = 5, 26.

2.5.3. Cell Cytotoxicity Evaluation of Gd/NIR-MSNs. HEK 293T cells were passaged when they are at confluence of 70% and inoculated to a 96-well plate (cell density 1×10^4 cells/well) in growth media (100 μL). Cells were cultured for 24 h before experiments. For the dose-dependent assay, Gd/NIR-MSNs were centrifuged and redispersed in fresh growth media and added to cultured cells to a final concentration of 0, 20, 40, 100, and 200 μg/mL. After 24 h of incubation at 37°C, supernatant was carefully removed and 100 μL medium and 20 μL MTT solution (5 mg/mL) were added and incubated for 4 additional hours. The supernatant in each well was aspirated and 150 μL dimethyl sulfoxide (DMSO) was added to solubilize cells and MTT crystals. After 4 h of shaking on a shaking table at room temperature and dark to dissolve all crystals, the blue color was read in a multiwall scanning spectrophotometer (ELx800, BioTek, USA) at a wavelength of 540 nm.

2.6. Animal Experiment

2.6.1. Animal Model. The animal study protocol was approved by the Animal Ethics Committee of Jinling Hospital. Female BALB/c nude mice (3-4 weeks old, 20–25 g) were purchased from the Comparative Medical Department of Jinling Hospital. U87-MG cells were harvested at 70% confluence and resuspended in PBS. Mouse tumor xenografts were established by U87-MG cells (2.0×10^6) inoculation into the right hind limbs of nude mice.

2.6.2. In Vivo Dual-Modal NIR and MR Imaging. U87-MG tumor bearing mice were anesthetized with 2% pentobarbital sodium and received an intratumor injection of 15 μL of Gd/NIR-MSNs PBS solution (5 mg/mL). MRI was conducted on a 3.0 T clinical MR scanner and a custom, premade four-channel mouse coil, using a coronal and transversal T_1 weighted sequence (TR = 670 ms, TE = 11 ms, Average = 4, Slice Thickness = 2.0 mm, FOV = 60 mm, and Flip Angle = 150). The nude mice were scanned before and after the intratumor injection of Gd/NIR-MSNs PBS solution (50 μL, 5 mg/mL). NIR imaging was performed using an IVIS Lumina XR system, with the emission collected at 808 nm and excited by the external laser at 778 nm. MR and NIR imaging were performed at different time points after injection (0, 4, 8, 24, and 48 h).

3. Results and Discussion

The synthesis procedures of the Gd/NIR-MSNs are shown in Figure 1. Firstly, MSNs-NH_2 were synthesized via a CTAB-directed sol-gel procedure by using TEOS and APTES as coprecursors. Secondly, CTAB was removed with ethanol and concentrated hydrochloric acid. Thirdly, NIR dye IR-808 and MR contrast agents Gd-DTPA were conjugated to MSNs-NH_2 simultaneously with condensation reaction between -NH_2 moieties of MSNs-NH_2 and -COOH groups of IR-808 as well as Gd-DTPA, resulting in the dual-modality imaging probes Gd/NIR-MSNs.

TEM images show that MSNs-NH_2 have a truncated-octahedral shape with a mean diameter about 120 nm (Figures 2(a)–2(c)). It was also observed that the particles consist of highly ordered mesostructure (Figure 2(b)). To further determine the porous features, nitrogen adsorption-desorption isotherm assay was conducted and uncovered a type IV isotherm according to the IUPAC nomenclature (Figure 2(d)). The sharp capillary condensation step and large hysteresis loop in the p/p_0 range of 0.45–1.0 reveal characteristics of mesoporous materials with a narrow pore size distribution. The pore size distribution calculated based on the nonlocal density functional theory (NLDFT) illustrated that MSNs-NH_2 have uniform mesopore size of 3 and 6 nm and a total pore volume of 0.53 $cm^3\ g^{-1}$.

After conjugation of IR-808 dyes and Gd-DTPA to MSNs-NH_2, BET results uncovered the nanoparticle surface area reduction from 473 m^2/g to 200 m^2/g, while the zeta potential is reduced from 32 ± 5 mV to 7.35 ± 5 mV. These features suggested the successful conjugation of the NIR and MR

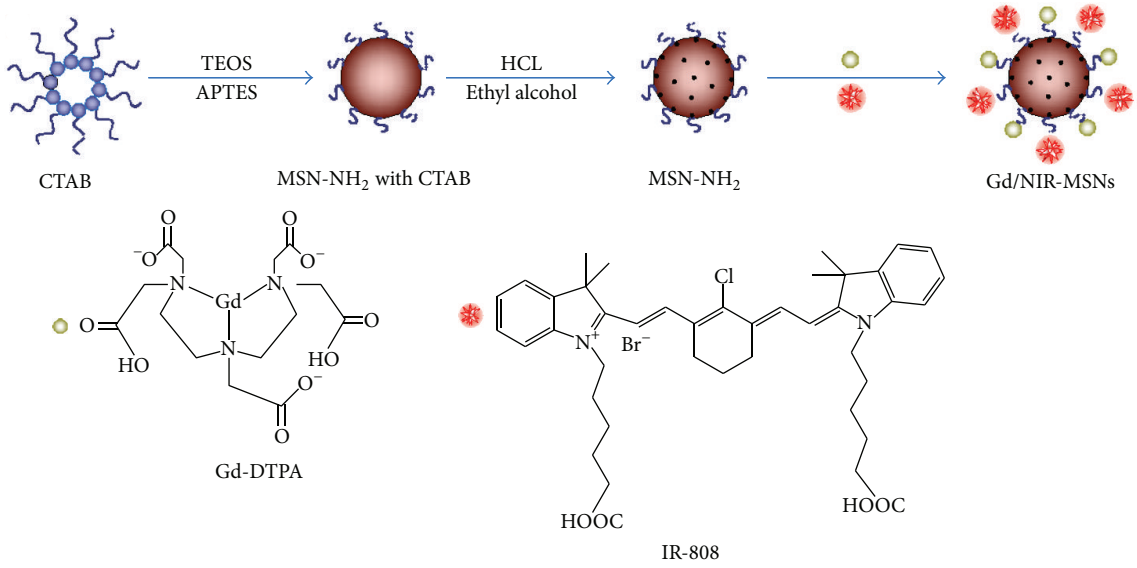

Figure 1: Schematic illustration of the synthesis procedures of the dual-modality imaging probes Gd/NIR-MSNs.

agents with MSN-NH_2. UV-vis absorption spectroscope and EDX spectrum measurement were also employed to confirm the presence of IR-808 and Gd-DTPA on Gd/NIR-MSNs particles. The absorption curve of Gd/NIR-MSNs illustrated a peak at 779 nm (Figure 2(e)), which is similar to the absorption peak of IR-808 and suggested the successful connection of IR-808 dyes with MSN-NH_2 [25]. Another peak documented by UV-vis absorption at 680 nm was also observed, which is attributed to Gd-DTPA on the particles. UV-vis absorption spectroscope analysis also showed that Gd/NIR-MSNs particles have an IR-808 dye loading amount of 0.3 wt%. EDX spectrum result provided direct evidence of Gd^{3+} presence on Gd/NIR-MSNs particles (Figure 2(f)), while ICP-AES measurements demonstrated 0.045 wt% conjugation amount for Gd-DTPA. The conjugation rate of Gd^{3+} is lower than previous report (3.42 wt%) [23, 26].

Strong fluorescence signals from NIR Gd/NIR-MSNs in deionized water were also identified (Figure 3(a)). The fluorescence emission spectra of the Gd/NIR-MSNs demonstrated a peak at 794 nm, which was similar with NIR dye IR-808 under the same condition [25]. These features suggesting the spectral properties of IR-808 are unchanged during the synthesis procedure, which will validate the potential ability of the bimodal probes for NIR imaging. As shown in Figure 3(b), in vitro phantom MRI study demonstrated a clear Gd^{3+} concentration dependent T_1 signal enhancement effect with a high r_1 value of 14.54 $mM^{-1}\,s^{-1}$. The relaxivity value is much larger than Gd-DTPA (4.75 $mM^{-1}\,s^{-1}$) under the same condition. The high magnitude relaxivities of Gd/NIR-MSNs are attributed to Gd^{3+} chelates attached to the mesochannels of the MSNs-NH_2, which makes readily accession and efficient relax of water protons through a reduction in the tumbling rate [10, 23].

Before proceeding to in vivo applications for NIR and MR dual-modal imaging, the uptake and retention ability of Gd/NIR-MSNs were evaluated in vitro with human glioblastoma cells U87-MG, which were stably transfected with green fluorescence protein. Figures 4(a)–4(d) demonstrated that the particles (red) distributed in the cytoplasm of U87-MG cells. TEM (Figure 4(e)) image further confirmed the uptake of the Gd/NIR-MSNs by the U87-MG cells. Biocompatibility is one of the most important prerequisites of nanoprobers for in vivo imaging. We chose human embryonic kidney cells HEK 293T to assess the cytotoxicity of Gd/NIR-MSNs with a MTT method. The results showed that no significant differences in the proliferation of the HEK 293T cells after 24 h of incubation with 20–200 μg/mL of Gd/NIR-MSNs (Figure 4(f)), suggesting the Gd/NIR-MSNs, have good biocompatibility.

To further investigate the biomedical dual-modality imaging ability of the probes, U87-MG cells were incubated with the Gd/NIR-MSNs before unndergoing NIR fluorescent and MR T_1 map imaging. U87-MG cells labeled with MSNs-NH_2 were treated as control. Strong NIR signal fluorescence was clearly visible in the optical image of tumor cells labeled with Gd/NIR-MSNs but completely absent in the image of cells incubated with MSNs-NH_2 (Figure 5(a)). Moreover, significant longitudinal relaxation time reduction was observed of cells labeled with Gd/NIR-MSNs on MR T_1 map image compared with control (Figure 5(b)), which suggested that robust T_1 enhancement can be achieved with the bimodal probes. These results validated the potential NIR and MR in vivo imaging ability of the Gd/NIR-MSNs.

In vivo experiments were performed on a rodent subcutaneous U87-MG glioblastoma modal to evaluate the dual-modal imaging effects of Gd/NIR-MSNs. NIR fluorescence and MR T_1 imaging were acquired at different time points (0, 4, 8, 24, and 48 h) after 50 μL of Gd/NIR-MSNs were intratumor injected (Figure 6). At 4 h after injection, the enhanced region on MR images were slightly augmented and showed a more homogeneous distribution with a distinction

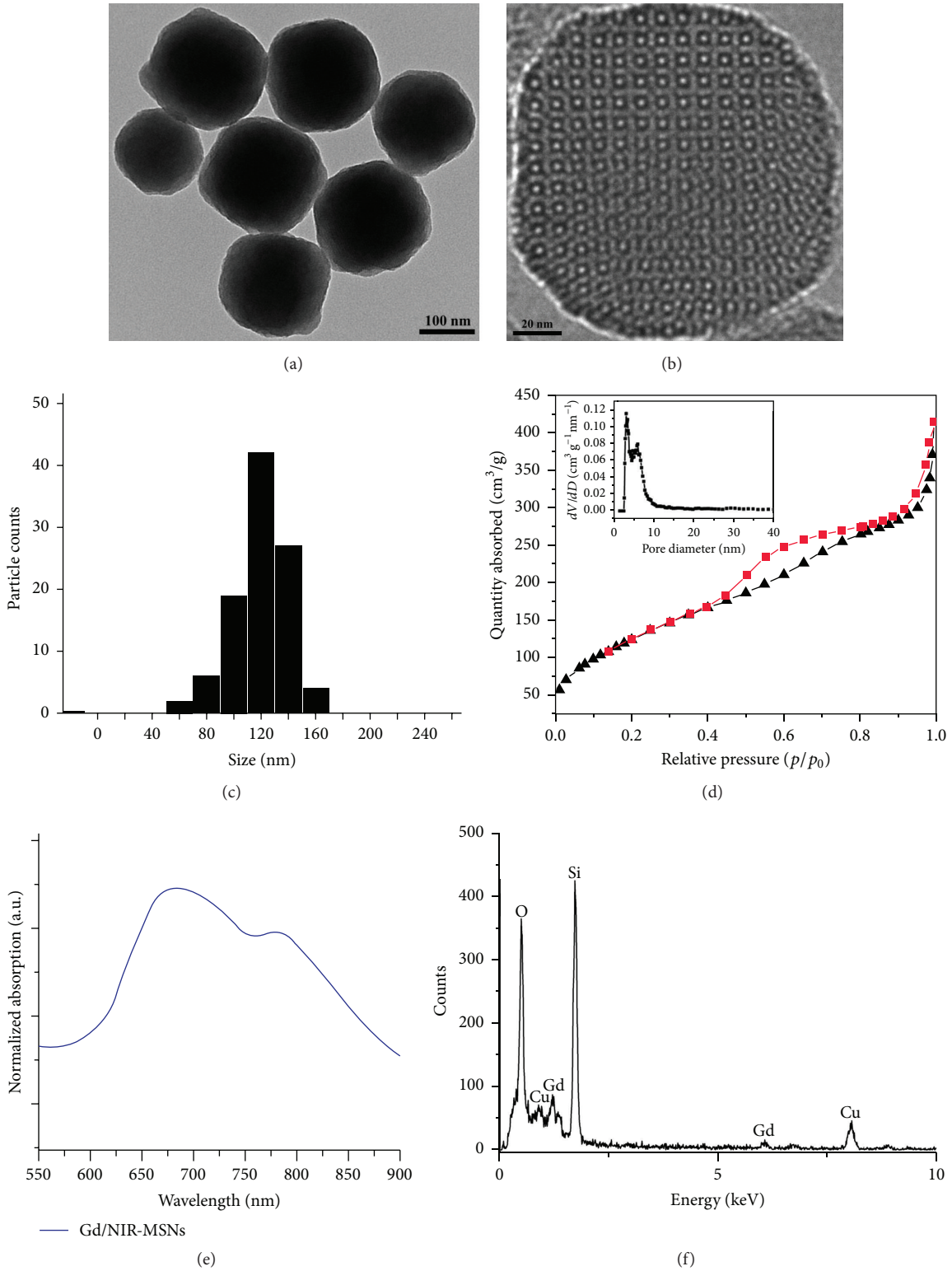

Figure 2: (a) and (b) TEM images of the highly aminated MSNs prepared by CTAB-directed sol-gel processes by using TEOS and APTES as coprecursors. (c) The particle size distribution of Gd/NIR-MSNs by counting about 100 particles on TEM images. (d) Nitrogen sorption isotherms and pore size distribution curve of the MSNs-NH_2. (e) The UV-vis absorption spectrum of the Gd/NIR-MSNs. (f) EDX spectrum of the Gd/NIR-MSNs.

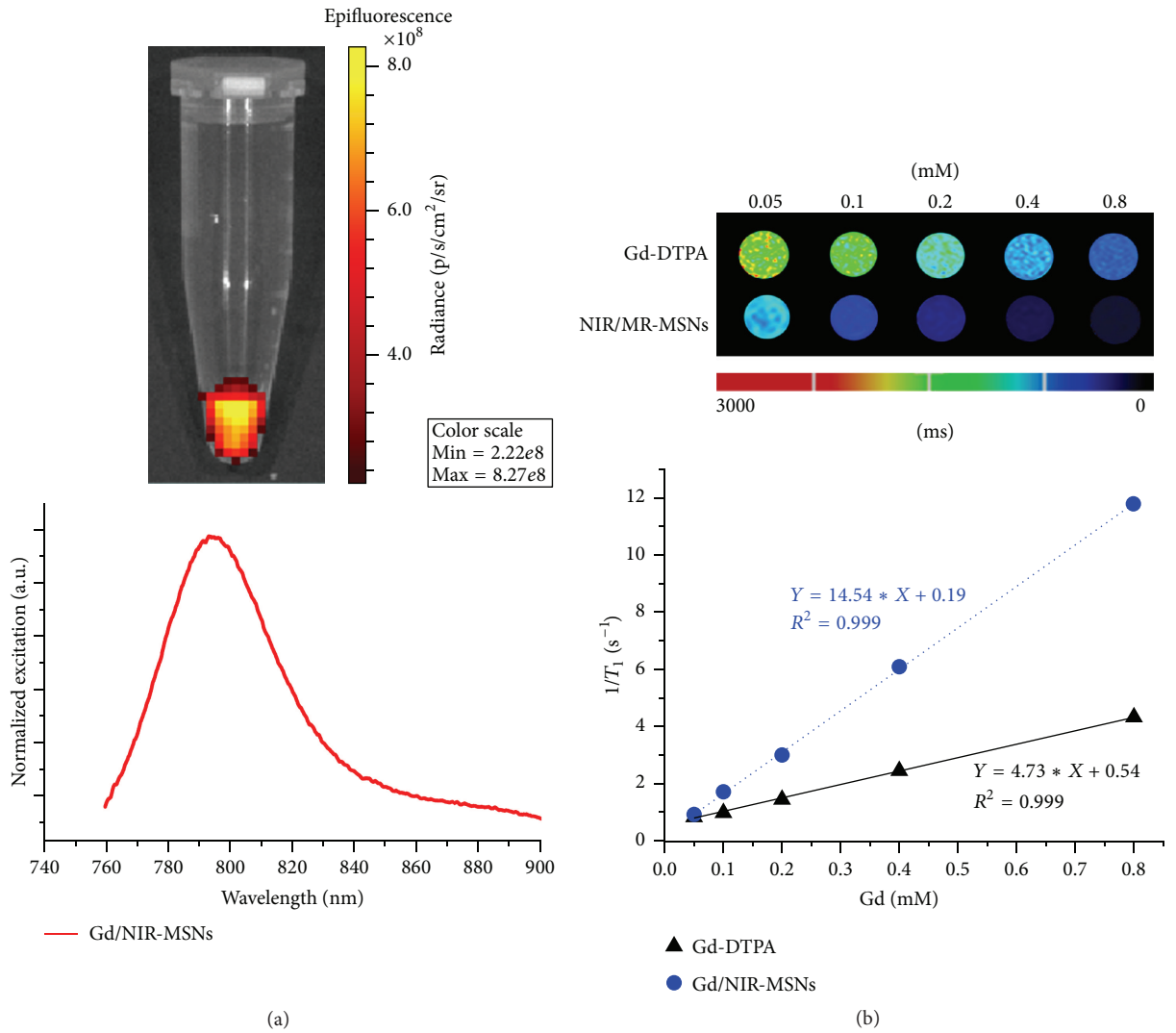

FIGURE 3: (a) NIR fluorescence imaging and emission spectra of the Gd/NIR-MSNs. (b) Phantom images and quantitative analysis of Gd/NIR-MSNs and Gd-DTPA by MR T_1 map examination.

margin of enhanced region, suggesting the excellent anatomic information provided by MR imaging (Figure 6(a)). And then, gradually MR T_1 signal reduction was observed over time (Figure 6(c)). At 48 h after injection, only slightly hyperintense T_1 signal remained in the tumor. The MR signal reduction is attributed to the diffusion of the nanoparticles. Figure S1 (in the Supplementary Material available online at http://dx.doi.org/10.1155/2016/6502127) shows the T_1 values (inversely proportional to signal intensity) at the injection region increase more quickly than the peripheral region, further confirming the diffusion of the nanoparticles in the tumor. For optical imaging, the NIR fluorescence signal showed a gradual augmentation over time and a poor signal margin due to the limitation of poor spatial resolution (Figures 6(b), 6(d) and Supplementary Figure S2 A). At the last time point of 48 h, there are still dramatic fluorescence signals that could be detected in the tumor region, which may be explained by the high sensitivity of optical imaging and the spreading of nanoparticles to the tumor surface. Hence, the imaging features revealed that MRI should be taken for high spatial resolution and anatomic images, while NIR fluorescent imaging should be used to provide high sensitivity lesion detection information. Combination of the two imaging modality could make excellent complementary for tumor detection and provide guidance for treatment.

4. Conclusions

In summary, we have successfully prepared a mesoporous silica nanoparticle based dual-modality probe (Gd/NIR-MSNs) by a facile protocol and carried out in vivo NIR fluorescence and MR imaging on a rodent tumor modal. The Gd/NIR-MSNs have uniform particle size about 120 nm and ordered mesostructure. Excellent biocompatibility and high intracellular retention ability of Gd/NIR-MSNs make it possible to be used as an in vivo imaging tool. Remarkable

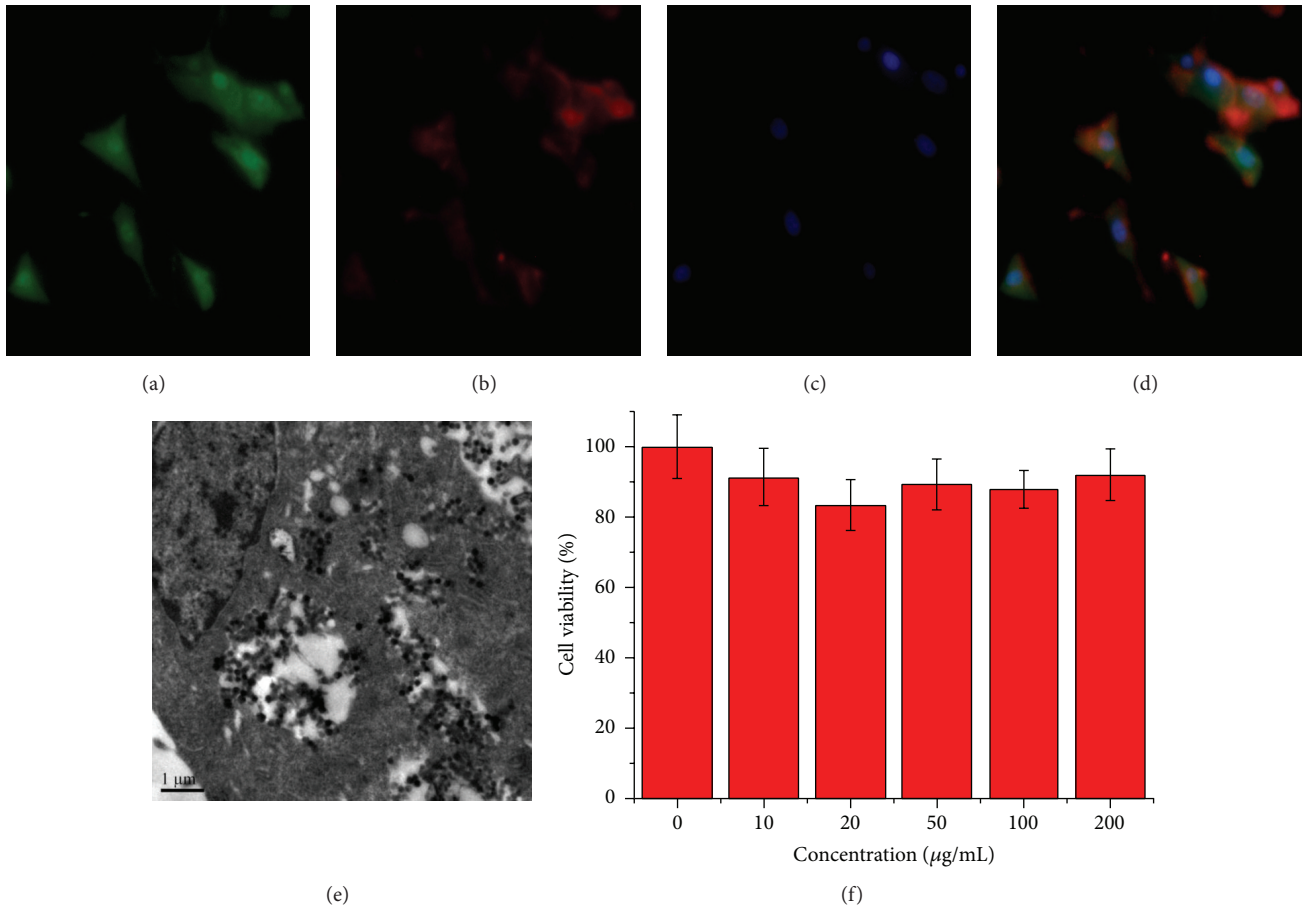

FIGURE 4: Cellular uptake of Gd/NIR-MSNs in human glioblastoma U87-MG-GFP cells. (a) GFP fluorescent image of U87-MG-GFP cells. (b) NIR fluorescent image of Gd/NIR-MSNs. (c) Nucleus staining of cells with DAPI. (d) The merged imaging of (a–c). (e) TEM image of the U87-MG-GFP cell incubated with the Gd/NIR-MSNs. (f) In vitro viability of human embryo kidney 293T cells incubated with Gd/NIR-MSNs.

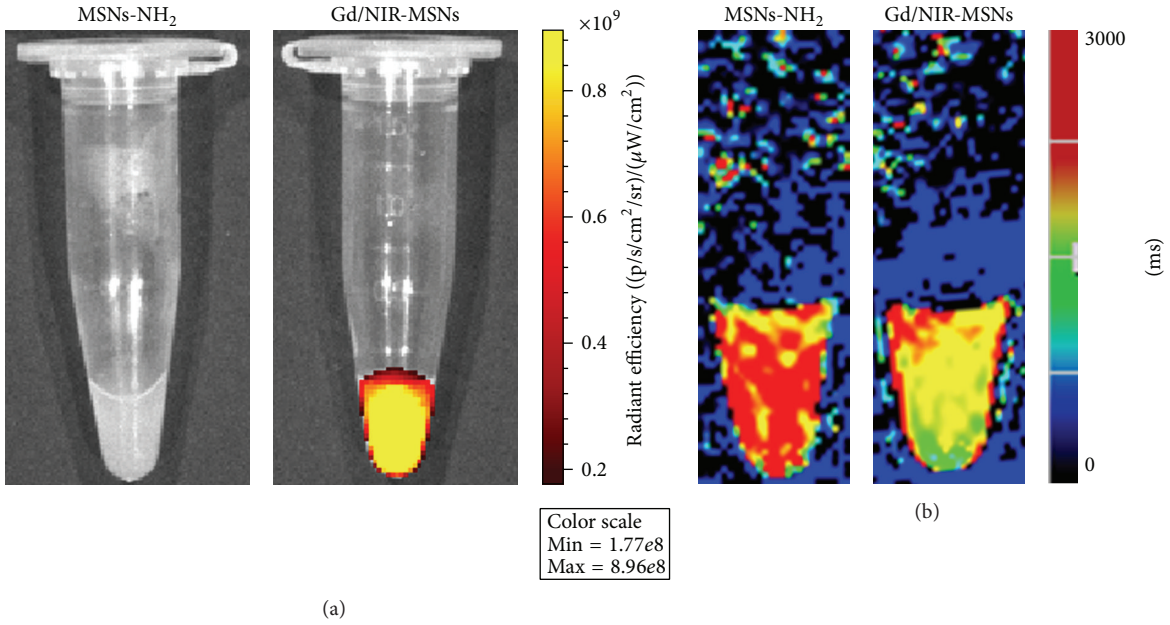

FIGURE 5: (a) NIR fluorescent and (b) MR T_1 map imaging of U87-MG cells labeled with MSNs-NH_2 and Gd/NIR-MSNs.

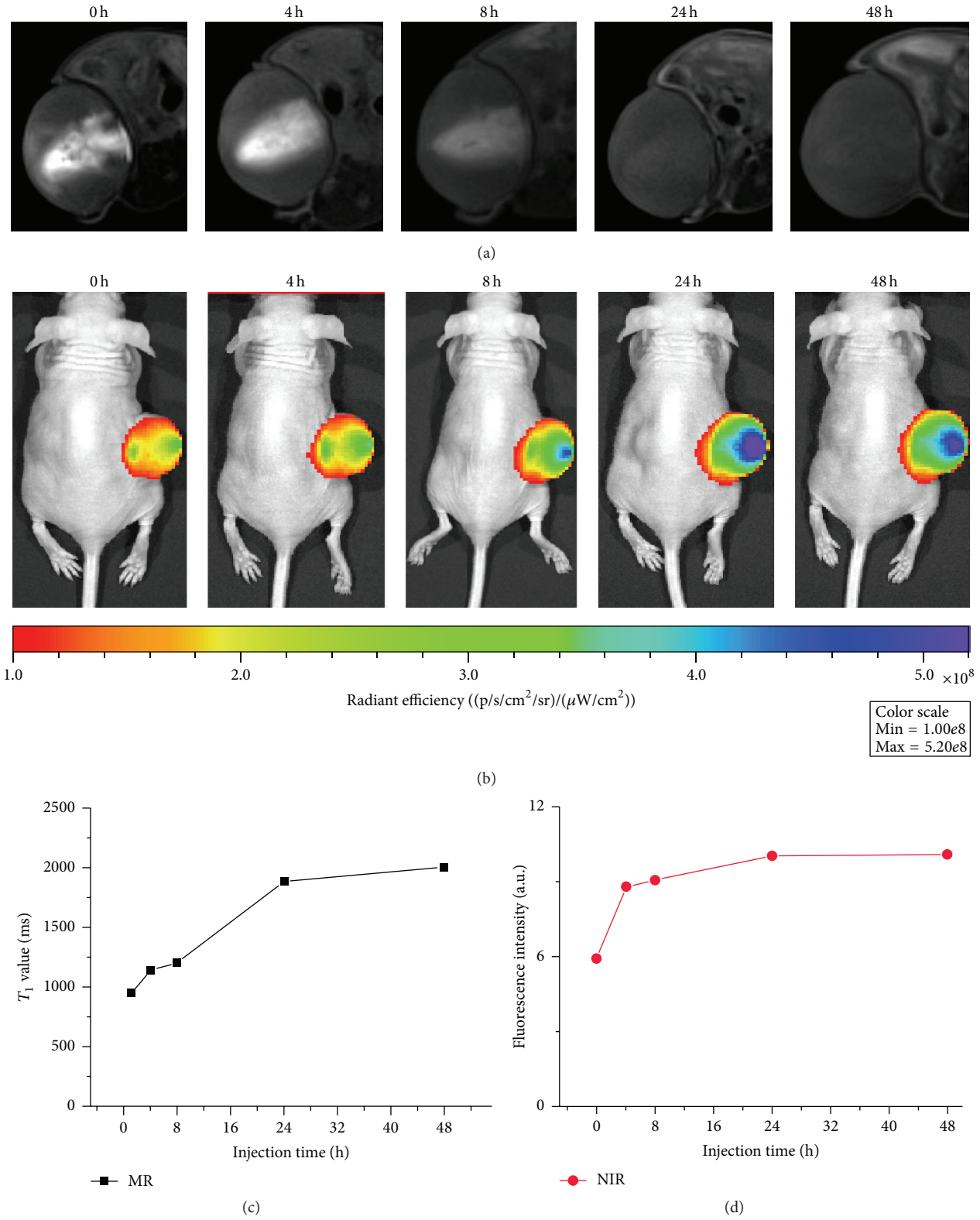

FIGURE 6: In vivo MR (a) and NIR florescence (b) dual-modality imaging of U87-MG tumor bearing mice model (coronal position) after intratumoral injection of Gd/NIR-MSNs at 0, 4, 8, 24, and 48 h. Quantitative analysis of the MR T_1 value (c) and NIR fluorescence intensity (d) in different time points.

NIR fluorescence property and highly MR T_1 relaxivity observed both in vitro and in vivo confirm the feasibility of Gd/NIR-MSNs as dual-modality imaging contrast agents in tumor detection. In addition, high sensitive images with distinct anatomical information are obtained by the Gd/NIR-MSNs, making the nanoprobes more potential for biomedical research.

Competing Interests

No potential competing interests were reported by the authors of this paper.

Acknowledgments

The authors thank the financial support from the National Key Basic Research Program of China (2014CB744504 and 2014CB744501), the Major International (Regional) Joint Research Program of China (81120108013), the National Natural Science Foundation of China (30930028, 81371622, 81471632, and 81371611), and China Postdoctoral Science Foundation (2015M581837).

References

[1] J. V. Jokerst and S. S. Gambhir, "Molecular imaging with theranostic nanoparticles," *Accounts of Chemical Research*, vol. 44, no. 10, pp. 1050–1060, 2011.

[2] B. Sharma, A. Martin, S. Stanway, S. R. D. Johnston, and A. Constantinidou, "Imaging in oncology-over a century of advances," *Nature Reviews Clinical Oncology*, vol. 9, no. 12, pp. 728–737, 2012.

[3] L. Duan, F. Yang, L. Song et al., "Controlled assembly of magnetic nanoparticles on microbubbles for multimodal imaging," *Soft Matter*, vol. 11, no. 27, pp. 5492–5500, 2015.

[4] R. Weissleder, "Molecular imaging in cancer," *Science*, vol. 312, no. 5777, pp. 1168–1171, 2006.

[5] S. Luo, E. Zhang, Y. Su, T. Cheng, and C. Shi, "A review of NIR dyes in cancer targeting and imaging," *Biomaterials*, vol. 32, no. 29, pp. 7127–7138, 2011.

[6] Y. Zhou, X. Liang, and Z. Dai, "Porphyrin-loaded nanoparticles for cancer theranostics," *Nanoscale*, In press.

[7] R. Weissleder and U. Mahmood, "Molecular imaging," *Radiology*, vol. 219, no. 2, pp. 316–333, 2001.

[8] C. Niu, Z. Wang, G. Lu et al., "Doxorubicin loaded superparamagnetic PLGA-iron oxide multifunctional microbubbles for dual-mode US/MR imaging and therapy of metastasis in lymph nodes," *Biomaterials*, vol. 34, no. 9, pp. 2307–2317, 2013.

[9] X. Huang, F. Zhang, S. Lee et al., "Long-term multimodal imaging of tumor draining sentinel lymph nodes using mesoporous silica-based nanoprobes," *Biomaterials*, vol. 33, no. 17, pp. 4370–4378, 2012.

[10] G. Tallec, P. H. Fries, D. Imbert, and M. Mazzanti, "High relaxivity and stability of a hydroxyquinolinate-based tripodal monoaquagadolinium complex for use as a bimodal MRI/optical imaging agent," *Inorganic Chemistry*, vol. 50, no. 17, pp. 7943–7945, 2011.

[11] J. L. Vivero-Escoto, R. C. Huxford-Phillips, and W. Lin, "Silica-based nanoprobes for biomedical imaging and theranostic applications," *Chemical Society Reviews*, vol. 41, no. 7, pp. 2673–2685, 2012.

[12] J. Zhou, Y. Sun, X. Du, L. Xiong, H. Hu, and F. Li, "Dual-modality *in vivo* imaging using rare-earth nanocrystals with near-infrared to near-infrared (NIR-to-NIR) upconversion luminescence and magnetic resonance properties," *Biomaterials*, vol. 31, no. 12, pp. 3287–3295, 2010.

[13] Y. Pan, L. Zhang, L. Zeng et al., "Gd-based upconversion nanocarriers with yolk–shell structure for dual-modal imaging and enhanced chemotherapy to overcome multidrug resistance in breast cancer," *Nanoscale*, vol. 8, no. 2, pp. 878–888, 2015.

[14] K. Chen, J. Xie, H. Xu et al., "Triblock copolymer coated iron oxide nanoparticle conjugate for tumor integrin targeting," *Biomaterials*, vol. 30, no. 36, pp. 6912–6919, 2009.

[15] F. Kiessling, J. Huppert, C. Zhang et al., "RGD-labeled USPIO inhibits adhesion and endocytotic activity of $\alpha v\beta 3$-integrin-expressing glioma cells and only accumulates in the vascular tumor compartment," *Radiology*, vol. 253, no. 2, pp. 462–469, 2009.

[16] O. Veiseh, C. Sun, J. Gunn et al., "Optical and MRI multifunctional nanoprobe for targeting gliomas," *Nano Letters*, vol. 5, no. 6, pp. 1003–1008, 2005.

[17] Z. Teng, S. Wang, X. Su et al., "Facile synthesis of yolk-shell structured inorganic-organic hybrid spheres with ordered radial mesochannels," *Advanced Materials*, vol. 26, no. 22, pp. 3741–3747, 2014.

[18] S. T. Selvan, "Silica-coated quantum dots and magnetic nanoparticles for bioimaging applications (Mini-Review)," *Biointerphases*, vol. 5, Article ID FA110, 2010.

[19] S. T. Selvan, T. T. Yang Tan, D. Kee Yi, and N. R. Jana, "Functional and multifunctional nanoparticles for bioimaging and biosensing," *Langmuir*, vol. 26, no. 14, pp. 11631–11641, 2010.

[20] Z. Teng, X. Su, Y. Zheng et al., "A facile multi-interface transformation approach to monodisperse multiple-shelled periodic mesoporous organosilica hollow spheres," *Journal of the American Chemical Society*, vol. 137, no. 24, pp. 7935–7944, 2015.

[21] J. L. Vivero-Escoto, K. M. L. Taylor-Pashow, R. C. Huxford et al., "Multifunctional mesoporous silica nanospheres with cleavable Gd(III) chelates as MRI contrast agents: synthesis, characterization, target-specificity, and renal clearance," *Small*, vol. 7, no. 24, pp. 3519–3528, 2011.

[22] P. Sharma, N. E. Bengtsson, G. A. Walter et al., "Gadolinium-doped silica nanoparticles encapsulating indocyanine green for near infrared and magnetic resonance imaging," *Small*, vol. 8, no. 18, pp. 2856–2868, 2012.

[23] K. M. L. Taylor, J. S. Kim, W. J. Rieter, H. An, W. Lin, and W. Lin, "Mesoporous silica nanospheres as highly efficient MRI contrast agents," *Journal of the American Chemical Society*, vol. 130, no. 7, pp. 2154–2155, 2008.

[24] T. Suteewong, H. Sai, R. Cohen et al., "Highly aminated mesoporous silica nanoparticles with cubic pore structure," *Journal of the American Chemical Society*, vol. 133, no. 2, pp. 172–175, 2011.

[25] X. Tan, S. Luo, D. Wang, Y. Su, T. Cheng, and C. Shi, "A NIR heptamethine dye with intrinsic cancer targeting, imaging and photosensitizing properties," *Biomaterials*, vol. 33, no. 7, pp. 2230–2239, 2012.

[26] Y.-Z. Shao, L.-Z. Liu, S.-Q. Song et al., "A novel one-step synthesis of Gd^{3+}-incorporated mesoporous SiO_2 nanoparticles for use as an efficient MRI contrast agent," *Contrast Media and Molecular Imaging*, vol. 6, no. 2, pp. 110–118, 2011.